

EFFECTS OF COSMIC INFRARED BACKGROUND ON HIGH-ENERGY DELAYED GAMMA-RAYS FROM GAMMA-RAY BURSTS

KOHTA MURASE¹, KATSUAKI ASANO², SHIGEHIRO NAGATAKI^{1,3}

Accepted for publication in ApJ

ABSTRACT

Regenerated high-energy emissions from gamma-ray bursts (GRBs) are studied in detail. If the intrinsic primary spectrum extends to the TeV range, these very high-energy photons are absorbed by the cosmic infrared background (CIB). Created high-energy electron-positron pairs up-scatter mainly cosmic microwave background (CMB) photons, and secondary photons are generated in the GeV-TeV range. These secondary delayed photons may be observed in the near future, which are useful for a consistency check of the intrinsic primary spectrum. In this paper, we focus on effects of the CIB on delayed secondary emissions. In particular, we show that not only up-scattered CMB photons but also up-scattered CIB ones are important, especially for low redshift bursts. They also give us additional information on the CIB, whose photon density is not definitely determined so far.

Subject headings: gamma rays: bursts — infrared: general — radiation mechanisms: non-thermal

1. INTRODUCTION

Gamma-ray bursts (GRBs) are highly relativistic astrophysical phenomena located at a cosmological distance. Observed gamma-ray spectra are typically highly nonthermal and extended to the MeV range or above. The relativistic shock scenario is one of the leading scenarios to reproduce such spectra (see reviews, e.g., (Mészáros 2006; Zhang 2007)). The internal shock model is one of widely accepted models. In this model, the GRB prompt emission is explained by electromagnetic radiation from relativistic electrons accelerated in shocks generated by collisions among the subshells. Theoretically, several emission mechanisms of GeV-TeV emission have been proposed. The synchrotron self-inverse Compton mechanism (SSC) is one of them (Papathanassiou & Mészáros 1996; Dai & Lu 2002; Guetta & Granot 2003; Peer & Waxman 2004; Casanova et al. 2007). While such models belong to leptonic scenarios, hadronic scenarios are also possible. In GRBs, protons can be accelerated up to the ultra high energy region. high-energy protons can not only radiate synchrotron photons (Totani 1998) but also produce electron-positron pairs, pions and muons via the photo-hadronic process (Waxman & Bahcall 1997; Asano 2005; Asano & Takahara 2003). Synchrotron radiation by electrons, positrons and muons can also contribute to resulting spectra (Dermer & Atoyan 2004; Asano & Inoue 2007). Neutrino detection would be strong evidence of baryon acceleration and expected by future neutrino detectors such as IceCube (Waxman & Bahcall 1997; Guetta et al. 2001; Guetta et al. 2004a; Dermer and Atoyan 2003; Murase & Nagataki 2006a; Asano & Nagataki 2006).

Sufficiently high-energy photons, including photons originating from protons, make pairs mainly via $\gamma\gamma \rightarrow e^+e^-$ interaction in the subshells and cannot escape from the source. As a result, the intrinsic high-energy cutoff of GRB spectra is usually determined by the optical depth for pair creation,

which largely depends on bulk Lorentz factors of subshells (Lithwick & Sari 2001; Razzaque et al. 2004). Even if such high-energy photons escape from the subshells, these photons may suffer from interactions with the cosmic infrared background (CIB) and be largely absorbed especially for high- z GRBs such as $z \gtrsim 1$. Hence, the detection of TeV photons will be very difficult, unless the GRB location is nearby. The secondary electron-positron pairs generated by attenuation are very energetic, so that they up-scatter numerous cosmic microwave background (CMB) photons by the inverse-Compton (IC) process. Such secondary photons will be observed as delayed GeV emissions (Cheng & Cheng 1996; Dai et al. 2002; Dai & Lu 2002; Guetta & Granot 2003; Wang et al. 2004; Razzaque et al. 2004; Ando 2004; Fan et al. 2004; Casanova et al. 2007). The delayed secondary emission is indirect evidence of the intrinsic TeV emission as well as a clue to probing the intergalactic magnetic (IGM) field (Plaga 1995). Such delayed secondary emission has been discussed in terms of not only the internal shock model but also the external shock model (Mészáros & Rees 1994; Mészáros et al. 1994; Dermer et al. 2000; Zhang & Mészáros 2001; Derishev et al. 2002; Wang et al. 2001; Wang et al. 2004; Ando 2004). They could be distinguishable by the distinct spectral evolution behavior.

Photon attenuation due to the CIB is very useful as an indirect probe of the CIB, whose photon density is not satisfactorily determined. The direct observation of the CIB is difficult, because of the bright foreground emission associated with zodiacal light as well as emission from our Galaxy. COBE DIRBE and COBE FIRAS have succeeded in highly significant detections of the residual diffuse infrared background, providing an upper bound on the CIB in the infrared regime. On the other hand, galaxy counts have given a lower bound on the CIB at wavelengths, where no COBE data are available. Despite the dramatic progress in observations achieved by Infrared Astronomical Satellite (IRAS), Infrared Space Observatory (ISO) and the Submillimeter Common-User Bolometric Array (SCUBA), the mid-infrared (MIR) and far-infrared (FIR) observations do not reach a level of optical and near-infrared (NIR) bands, which can be explained by direct stellar emission. In this sense, we have not determined the spectral

¹ YITP, Kyoto University, Kyoto, Oiwake-cho, Kitashirakawa, Sakyo-ku, Kyoto, 606-8502, Japan

² Division of Theoretical Astronomy, NAOJ, Osawa 2-21-1, Mitaka, Tokyo, 181-8588, Japan

³ KIPAC, Stanford University, P.O. Box 20450, MS 29, Stanford, CA, 94309, USA

energy distribution (SED) of the CIB with sufficient accuracy yet. For recent reviews, see Hauser & Dwek (2001) and Kashlinsky (2006). Stecker et al. (1992) proposed that one can use photon attenuation in blazars to determine the intensity of the CIB, if we know intrinsic spectra of blazars. Subsequent studies used observations of TeV emissions from blazars (for one of the latest examples, Aharonian et al. (2006)). Conversely, we could obtain information on the intrinsic primary spectrum such as the intrinsic high-energy cutoff, if we know the CIB accurately. Similarly to cases of blazars, we can expect to make use of GRBs as a probe of the CIB. However, owing to uncertainties in GRB intrinsic spectra, the depletion due to the CIB in high-energy spectra is hard to be estimated.

Observationally, GeV photons have been detected from some GRBs with the EGRET detector on the Compton Gamma-Ray Observatory. Especially, EGRET detected prolonged GeV emission from GRB 940217 (Hurley et al. 1994) and GRB 930131 (Sommer et al. 1994). Although we do not know the highest energy in GRB spectra observationally, theoretical consideration and simple extrapolation of GRB spectra enable us to expect TeV photons from some GRBs. Furthermore, the tentative detection of an excess of TeV photons from GRB 970417a at the 3σ level has been claimed with a chance probability $\sim 1.5 \times 10^{-3}$ by the water Čerenkov detector Milagro (Atkins et al. 2000), although Milagro has not observed such signals so far (Milagro Collaboration 2007). Another possible TeV detection of GRB 971110 has been reported with the GRAND array at the 2.7σ level (Poirier et al. 2003). Staking of data from the TIBET array for a large number of GRB time window has led to an estimate of a $\sim 7\sigma$ composite detection significance (Amenomori et al. 2001). Further observations of such very high-energy gamma-ray signals by MILAGRO, MAGIC (Mirzoyan et al. 2005), VERITAS (Holder et al. 2006), HESS (Hinton 2004) and CANGAROOIII (Enomoto et al. 2002) might enable us to detect the signals in the near future. However, the photon detection in the TeV range can be expected only for nearby events, since high-energy gamma-rays will suffer from attenuation by the CIB. On the other hand, future detectors such as Gamma-Ray Large Area Space Telescope (GLAST) will detect many GRBs around the GeV range. They will also enable us to discuss not only prompt primary emissions but also delayed secondary emissions produced via IC up-scattering.

It depends on the strength of IGM field whether we can observe such delayed gamma-ray signals or not. For electron-positron pairs produced by attenuation of 1 TeV primary photons, the sufficiently strong IGM field $B \gtrsim 10^{-16}$ G leads to the large magnetic deflection of pairs, $\theta_B \gtrsim 1$, and long time delay of secondary photons, $\Delta t_B \gtrsim 10^3$ s, so that the secondary gamma-ray flux will be suppressed. On the other hand, the weak IGM field enables us to have possibilities to detect delayed secondary gamma-ray signals. In this paper, we study these two extreme cases, the weak IGM field case and strong IGM field case. In the former case, the magnetic deflection time is not so important and other time scales such as the angular spreading time scale are more important for relevant energies. In the latter case, it becomes difficult to observe delayed secondary gamma-rays directly from each burst, but they contribute to the diffuse gamma-ray background.

In this paper, we study delayed secondary gamma-ray spectra from GRBs most quantitatively by numerical simulations as well as an approximate formula. We focus on effects of the

CIB by including the contribution from up-scattered CIB photons (hereafter, USIB photons) to delayed secondary spectra, which can extend delayed spectra to higher energies but has not been emphasized in previous studies. Such a study would be important for GRBs that can emit \sim TeV emissions in order to know the intrinsic feature of the source. In addition, it would be useful to obtain information on the CIB more quantitatively. Not only GLAST but also MAGIC and VERITAS might detect up-scattered CIB photons in the near future.

This paper is structured as follows. In §2.1, we explain the models of intrinsic GRB spectra and we describe the delayed emission mechanism in §2.2. The CIB model we use in this paper is explained in §2.3. We show the method to estimate the diffuse gamma-ray background due to GRBs in §2.4. In §3, we show the results. Finally, our summary and discussion are described in §4.

2. THE MODEL

2.1. Model of Intrinsic Spectra

Throughout the paper, we focus on long GRBs with the typical duration $T \sim 10 - 100$ s. Widths of individual pulses vary in a wide range. Typical pulses have the duration with $\delta t \sim 0.1 - 10$ s and shortest spikes have millisecond or even sub-millisecond widths. The internal shock model, in which gamma-rays arise by the internal dissipation of relativistic jets, can reproduce such wide range variability. However, the simple synchrotron model cannot explain several properties of prompt emission (see, e.g., Mészáros 2006). In this paper, we do not consider these open problems on the prompt emission mechanism. The observed photon spectrum is well approximated by a broken power-law, $dN_\gamma/dE_\gamma \propto (E_\gamma/E_\gamma^b)^{-\alpha}$ for $E_\gamma^{sa} < E_\gamma < E_\gamma^b$ and $dN_\gamma/dE_\gamma \propto (E_\gamma/E_\gamma^b)^{-\beta}$ for $E_\gamma^b < E_\gamma < E_\gamma^{max}$, where E_γ^{sa} is the synchrotron self-absorption cutoff, and E_γ^{max} is the intrinsic high-energy cutoff.

The intrinsic high-energy cutoff E_γ^{max} is typically determined by the opacity of two-photon annihilation into an electron-positron pair. In the internal shock scenario, it is easy to see that TeV photons can escape from the subshells if an internal collision radius and/or a bulk Lorentz factor are large enough (Lithwick & Sari 2001).

In sufficiently high-energy ranges, gamma-rays due to electron SSC, proton synchrotron and charged-meson/muon synchrotron can contribute to intrinsic spectra via cascade processes. The resulting spectra are complicated and the study on them is beyond scope of this paper. We will investigate not the intrinsic emission but the delayed emission in detail. The delayed emission depends on the amount of attenuated photons and would not be so sensitive to the detail of the shape of intrinsic spectra with a given E_γ^{max} . Throughout the paper we adopt three models with total isotropic energy $E_{iso} = 10^{53}$ ergs for calculation. Model A: a broken-power law spectrum with $\alpha = 1$ and $\beta = 2.2$, $E_\gamma^b = 300$ keV and $E_\gamma^{max} = 1$ TeV. Model B: the same as model A but $E_\gamma^{max} = 10$ TeV. Model C: a numerically calculated spectrum obtained by Asano & Inoue (2007). They perform Monte Carlo simulations including synchrotron radiation, Compton scattering, pair creation, synchrotron self-absorption and particles originating from protons such as electrons, positrons, muons and pions. We adopt one of their numerical results as model C. For details, see Asano & Inoue (2007). Parameters adopted to obtain the spectrum in model C are energy per subshell $E_{sh} = 10^{50}$ ergs, $E_\gamma^b = 300$ keV, an internal collision radius $r = 10^{15}$ cm and a Lorentz

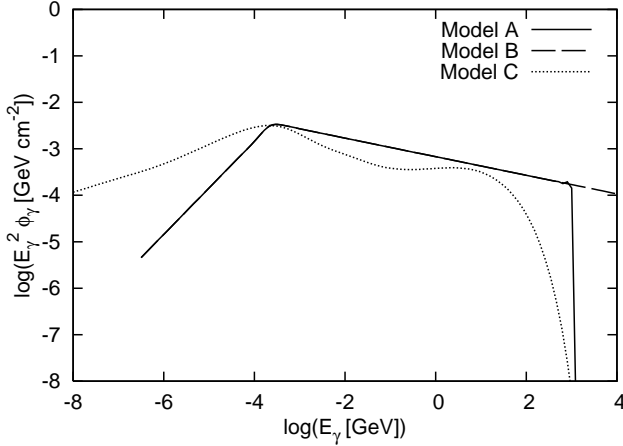


FIG. 1.— The intrinsic primary spectra we use in this paper for each model. The spectra are normalized by the fluences from a source at $z = 1$. Model parameters are described in the text.

factor $\Gamma = 100$. The magnetic energy density U_B is assumed to be $0.1U_\gamma$, where U_γ is the photon energy density in the subshell. In Fig. 1, we show the intrinsic spectra for the three models we adopt. The second peak of model C in Fig. 1 is due to SSC. Above this peak energy, photon absorption due to pair creation is crucial. The intrinsic GRB duration (defined in the local rest frame) is set to $T' = 50$ s.

2.2. Delayed Emission

For typical GRBs at the source redshift $z = 1$, most high-energy photons above ~ 70 GeV produce electron-positron pairs. The produced high-energy pairs cause delayed high-energy photon emission via IC up-scattering of CMB and CIB photons. The duration of such delayed emission is determined by several effects (Dai et al. 2002; Dai & Lu 2002; Wang et al. 2004; Razzaque et al. 2004; Ando 2004; Fan et al. 2004); the angular spreading, IC cooling and magnetic deflection effects. The angular spreading time is expressed as,

$$\Delta t_{\text{ang}} \approx (1+z) \frac{\lambda_{\gamma\gamma}}{2\gamma_e^2 c} \quad (1)$$

where γ_e is the Lorentz factor of secondary electrons or positrons in the local rest frame in the Robertson-Walker metric (hereafter, the local rest frame) at each z , and $\lambda_{\gamma\gamma}$ is the photon mean free path. The IC cooling time scale is written as,

$$\Delta t_{\text{IC}} \approx (1+z) \frac{\hat{t}_{\text{IC}}}{2\gamma_e^2} \quad (2)$$

where \hat{t}_{IC} is the cooling time scale in the local rest frame. If the magnetic deflection angle is sufficiently small, the magnetic deflection time is,

$$\Delta t_B \approx (1+z) \frac{1}{2} \hat{t}_{\text{IC}} \theta_B^2 \quad (3)$$

where $\theta_B = \hat{t}_{\text{IC}}/r_L$ is the magnetic deflection angle and r_L is the Larmor radius of electrons or positrons. Note that we have implicitly assumed $1/\gamma_e, \theta_B \ll \theta_j$ where θ_j is an opening angle of GRB jet. Taking into account the GRB duration T , the (secondary) duration time scale is estimated by the maximum time scale, $\Delta t = \max[\Delta t_{\text{ang}}, \Delta t_{\text{IC}}, \Delta t_B, T]$. Examples of Δt adopting the CIB model of Kneiske et al. (2004, see section 2.3) are shown in Fig. 2. In cases with a weak magnetic field such as $B \lesssim 10^{-(18-19)}$ G, the angular spreading time scale is

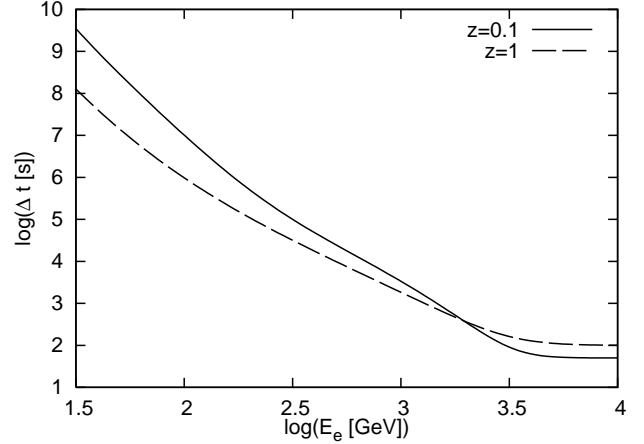


FIG. 2.— The maximum time scales for $z = 0.1$ and $z = 1$ involved in calculating the delayed secondary spectra. E_e is the electron energy in the local rest frame. The IGM field is assumed to be $B = 10^{-20}$ G.

the most important. Of course, we should note that we treat the averaged flux over the duration time scale.

The IGM field make the situation complicated and more careful treatments would be needed to evaluate the accurate time-dependent flux of delayed emission. The delayed emission can also be a probe of the IGM field (Plaga 1995), but we do not focus on this topic in this paper. We will treat the two extreme cases. One is the weak IGM field case, where we can expect detectable delayed secondary gamma-ray signals from GRBs. For demonstration, we use an IGM field with $B = 10^{-20}$ G, in which Δt_B is not so important. The other is the strong IGM field case, where it becomes difficult to detect delayed signals directly from each GRB. We will consider this case later.

Let us use the local approximation that TeV gamma-rays from a GRB interact with the CIB field at the same redshift, which is justified by numerical calculations later. We can obtain delayed spectra from a burst with the source redshift z by an analytic approximate formula, which is given by (Blumenthal & Gould 1970; Dai et al. 2002; Wang et al. 2001; Razzaque et al. 2004; Ando 2004; Fan et al. 2004),

$$\frac{dF_\gamma}{dt dE_\gamma}(E_\gamma, t, z) = \int_0^t dt_p \int d\varepsilon \int_{\gamma_e^{\text{min}}}^{\gamma_e^{\text{max}}} d\gamma_e \left(\frac{dF_e}{dt_p d\gamma_e} \right) \times \left(\frac{dN_\gamma}{dE_\gamma d\varepsilon d\hat{t}_d} \right) e^{-\tau_{\gamma\gamma}^{\text{bkg}}(E_\gamma, z) \hat{t}_{\text{IC}}} \frac{e^{-(t_d/\Delta t)}}{\Delta t}, \quad (4)$$

where the electron injection spectrum

$$\frac{dF_e}{dt_p d\gamma_e}(E_e, t_p, z) = 2 \frac{dE_{\gamma,i}}{d\gamma_e} \frac{dF_{\gamma,i}}{dE_{\gamma,i} dt_p}(E_{\gamma,i}, t_p, z) \times (1 - e^{-\tau_{\gamma\gamma}^{\text{bkg}}(E_{\gamma,i}, z)}), \quad (5)$$

and the photon emission spectrum per unit time due to IC scat-

tering

$$\begin{aligned} \frac{dN_\gamma}{dx d\varepsilon dt_d} &= \frac{2\pi r_0^2 m_e c^3}{\gamma_e} \frac{1}{\varepsilon} \frac{dn}{d\varepsilon}(\varepsilon, z) \left[2y \ln(2y) \right. \\ &\quad \left. + (1+2y)(1-y) + \frac{(wy)^2}{2(1+wy)}(1-y) \right], \\ x &\equiv \frac{E_\gamma(1+z)}{\gamma_e m_e c^2}, \\ y &\equiv \frac{x m_e c^2}{4\varepsilon \gamma_e (1-x)}, \\ w &\equiv \frac{4\varepsilon \gamma_e}{m_e c^2}. \end{aligned} \quad (6)$$

Here, $dF_{\gamma,i}/dE_{\gamma,i}dt_p$ is the intrinsic primary gamma-ray spectrum of GRB prompt emission, $E_{\gamma,i} = 2\gamma_e m_e c^2/(1+z)$ is energy of primary photons (where the source redshift is taken into account), $dn/d\varepsilon$ is the photon density spectrum of the CMB and CIB in the local rest frame, and r_0 is the classical electron radius. t is the given observation time of the delayed emission, t_p is the time when primary photons are released, T is the GRB duration, t_d is defined by $t_d = t - t_p$ and $\tau_{\gamma\gamma}^{\text{bkg}}(E_\gamma, z)$ is the optical depth against gamma-rays propagating in the universe. The upper bound of the integration over γ_e is determined by the high-energy cutoff of the intrinsic primary emission, i.e., $\gamma_e^{\text{max}} = (1+z)E_\gamma^{\text{bkg}}/2$. On the other hand, the lower bound of the integration over γ_e is $\gamma_e^{\text{min}} = \max[m_e c^2/2\varepsilon, ((1+z)E_\gamma/\varepsilon)^{1/2}/2]$. We exploit Eq. (4) iteratively by substituting $(dF_\gamma/dt dE_\gamma)(\exp(\tau_{\gamma\gamma}^{\text{bkg}}) - 1)$ into $dF_{\gamma,i}/dt_p dE_{\gamma,i}$ instead of using the intrinsic primary flux. We perform such an iterative method in order to include IC scattering by generated pairs due to re-absorbed secondary photons.

In the above formula, it is assumed that secondary pairs are produced only at the source redshift and cooling time scales are evaluated with quantities at the source redshift. The photon emission spectrum is evaluated with the initial energy of secondary pairs and assumed to be constant while the pairs cool. However, pairs are produced at various redshifts and the cooling rate becomes lower as they cool. Therefore, we also execute numerical simulations including IC scattering and pair creation. Based on the pair creation rate at each redshift due to the CIB (partially CMB), we follow the time evolution of the distribution functions of primary photons $f_\gamma(E_{\gamma,i})$, secondary pairs $f_e(\gamma_e)$, and secondary photons $f_2(E_\gamma)$ from the burst time to the present time. The minimal time (redshift) step for $f_\gamma(E_{\gamma,i})$ in our simulation is $dz = 0.005$. The pair cooling process is followed with a time step $\hat{t}_{\text{IC}}/100$ until pairs become non-relativistic. While $f_\gamma(E_{\gamma,i})$ decreases monotonically with time (or remains constant for lower energy range) by attenuation, $f_2(E_\gamma)$ does not necessarily change monotonically especially for high-redshift sources, because of re-absorption. IC photon spectra are calculated using the Klein-Nishina cross section with the Monte Carlo method used in (Asano 2005). Our method can precisely treat re-absorption of secondary photons and energy loss processes of electron-positron pairs.

2.3. Cosmic Infrared Background

Gamma-ray absorption due to pair creation in cosmological scales depends on the line-of-sight integral of the evolving density of low energy photons in the universe. To

demonstrate the effect of the CIB on delayed spectra from GRBs, we need to exploit some model of the CIB. The CIB should be explained by a theory from the first principles, but we are far from this ultimate goal owing to poor knowledge about star formation, supernova feedback, galaxy merging and so on. So far many models of SED of the CIB produced by stellar emission and dust re-radiation in galaxies have been constructed (Totani & Takeuchi 2002; Kneiske et al. 2002; Stecker et al. 2006). At lower redshifts, these models agree with each other basically. At higher redshifts, Stecker et al. (2006) found the larger optical depths than previously thought because of intergalactic gamma-ray absorption motivated by the recent discovery of active star formation taking place in young galaxies at high redshifts. Such model uncertainties will produce corresponding differences.

In this paper, we use the CIB model developed by Kneiske et al. (2002, 2004). They developed the evolving model of the infrared-to-ultraviolet metagalactic radiation field, based directly on observed emissivities. They specially addressed the redshift evolution of the SEDs, which are constructed from realistic stellar evolution tracks combined with detailed atmospheric models (Bruzual & Charlot 1993), and also taken into account effects of re-radiation from dusts and Polycyclic Aromatic Hydrogen molecules in the infrared. Their model parameterizes the main observational uncertainties, the redshift dependence of the cosmic star formation rate and the fraction of UV radiation released from the star forming regions. Here, we adopt the “best-fit model” of Kneiske et al. (2004), which is consistent with the data obtained from recent galaxy surveys. In Fig. 3, we show the SED of the CMB+CIB we use in this paper. For details, see Kneiske et al. (2002, 2004). We also assume the Λ CDM cosmology with $\Omega_m = 0.3$, $\Omega_\Lambda = 0.7$ and $H_0 = 70 \text{ km s}^{-1} \text{ Mpc}^{-1}$.

Given the SEDs, we can calculate the mean free path of high energy gamma-rays for pair creation or pair creation rate at each redshift. Especially, using the cross section of pair creation $\sigma_{\gamma\gamma}$, the optical depth of the universe is written as,

$$\tau_{\gamma\gamma}^{\text{bkg}} = \int_0^z dz \left| \frac{cdt}{dz} \right| \int d\cos\theta \frac{1-\cos\theta}{2} \int d\varepsilon \frac{dn}{d\varepsilon} \frac{d\sigma_{\gamma\gamma}}{d\cos\theta}(E_\gamma, \theta, \varepsilon) \quad (7)$$

For details, see Kneiske et al. (2004). For reference, we plot optical depths at $z = 0.1$ for the other models in Fig. 4. Note that the simple power-law fitting formula of Casanova et al. (2007) overestimates optical depths in comparison with the

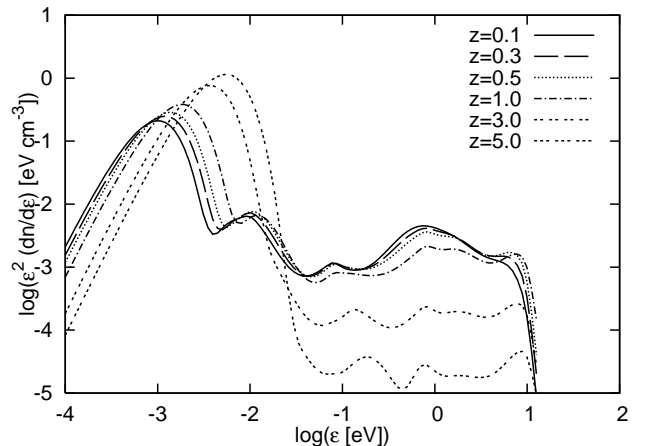


FIG. 3.— The CMB+CIB radiation field in the comoving frame for various redshifts, which we have used in this paper. The data about the CIB field are taken from the best-fit model of Kneiske et al. (2004)

other models above $\sim \text{TeV}$.

2.4. Diffuse Gamma-Ray Background

As noted before, if the IGM field is strong enough ($B \gtrsim 10^{-16} \text{ G}$), it is hard to detect delayed emissions as a source connecting with GRB prompt emissions because of large Δt_B . Therefore, such emissions may be detected as the diffuse gamma-ray background emission rather than delayed emissions. Now, we consider this extreme case.

The observed diffuse gamma-ray emission was found to be a power-law in energy and is highly isotropic on the sky (Sreekumar et al. 1998), but it may not be consistent with a simple power-law and The origin of the diffuse gamma-ray background from extragalactic sources is also an open question. Blazar is one of the most discussed and promising candidates. Other sources such as fossil radiation from accelerated cosmic rays during the structure formation might give a significant contribution. GRB is one of the brightest astrophysical phenomena and also can contribute to the gamma-ray background. GRBs as sources for the $\sim \text{MeV}$ gamma-ray background were given by Hartmann et al. (2002). Casanova et al. (2007) considered GRBs as sources of the $\sim \text{GeV-TeV}$ gamma-ray background. However, since GRBs are rare phenomena despite of their brightness, the contribution to the gamma-ray background will be small, as is shown later.

We estimate the diffuse gamma-ray background, independently of the IGM, as follows. The number of GRBs is written as,

$$\dot{N}_{\text{GRB}} = \int_{z_{\min}}^{z_{\max}} dz \frac{\rho_{\text{GRB}}(z)}{1+z} \frac{dV}{dz}, \quad (8)$$

where the volume factor

$$\frac{dV}{dz} = \frac{c}{H_0} \frac{4\pi d_L^2}{(1+z)^2 \sqrt{\Omega_m(1+z)^3 + \Omega_\Lambda}}, \quad (9)$$

(d_L is the luminosity distance) and the GRB rate

$$\rho_{\text{GRB}}(z) = \rho_0 \frac{23e^{3.4z}}{22 + e^{3.4z}} \frac{\sqrt{\Omega_m(1+z)^3 + \Omega_\Lambda}}{(1+z)^{3/2}}. \quad (10)$$

Here, we have used the SF2 model of Porciani & Madau (2001) for the GRB rate with $\rho_0 = 1 \text{ Gpc}^{-3} \text{ yr}^{-1}$, assuming that the GRB rate traces the star formation rate in a global sense. Guetta et al. (2004) obtained such a value of the GRB rate and Liang et al. (2007) also reported a similar value. Even though

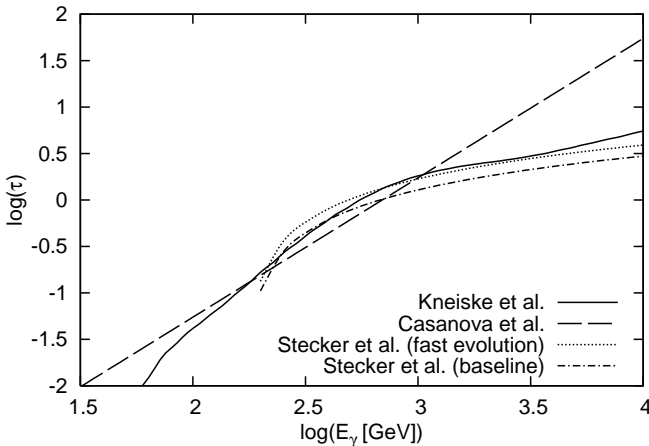


FIG. 4.— The optical depth of high-energy gamma-rays from a source at $z = 0.1$.

the actual GRB rate may not be a good tracer of the star formation rate (Guetta & Piran 2007; Le & Dermer 2007), our conclusion about the diffuse background would not be changed so much because the main contribution to the background comes from bursts that occur at $z \sim (1-2)$, the number of which is observationally determined. The diffuse gamma-ray background due to GRBs is estimated by,

$$\frac{dF_\gamma}{dE_\gamma} = \int_{z_{\min}}^{z_{\max}} dz \left(\frac{dN_\gamma}{dE_\gamma dA} \right) \frac{d\dot{N}_{\text{GRB}}}{dz} \quad (11)$$

where $dN_\gamma/dE_\gamma dA$ is the observed gamma-ray fluence from each burst, which is defined by,

$$\frac{dN_\gamma}{dE_\gamma dA} \equiv \frac{1}{4\pi d_p^2} \frac{dN_\gamma}{dE_\gamma}, \quad (12)$$

where dN_γ/dE_γ is the photon number spectrum (where the source redshift is taken into account) and d_p is the proper distance to a source. We set $z_{\min} = 0$ and $z_{\max} = 5$.

We have to note that TeV emissions from GRBs in the internal shock model can be expected only in the limited cases. In the context of the internal shock model, a sufficiently large Lorentz factor and/or large collision radius are required. Although a fraction of such GRBs that can emit TeV gamma-rays is unknown, maybe only a fraction of GRBs are TeV emitters. Hence, the contribution of GRBs to the diffuse gamma-ray background would give an upper limit, since it is evaluated under the assumption that all GRBs have spectra extended to TeV energies.

3. RESULTS

3.1. Delayed Gamma-Ray Spectra

In Figs. 5 and 6, we show total fluences of prompt and delayed gamma-rays numerically calculated for various redshifts. In model A ($E_\gamma^{\max} = 1 \text{ TeV}$), the maximum energy of secondary pairs is at most $\sim 500 \text{ GeV}$ in the local rest frame. Hence, the typical energy of up-scattered CMB photons (hereafter, USMB photons) is $\sim 1 \text{ GeV}$, above which USIB photons can make significant contributions to resulting delayed spectra. Such USIB photons form a relatively flat “slope” in spectral shape in the $\sim (10-100) \text{ GeV}$ range for $z \lesssim 3$. For $z \gtrsim 3$, such high-energy slope signature becomes difficult to be seen, because secondary photons are absorbed again.

The above picture is changed, if E_γ^{\max} is beyond 1 TeV . For model B ($E_\gamma^{\max} = 10 \text{ TeV}$), the maximum energy of secondary pairs is $\sim 5 \text{ TeV}$ in the local rest frame. Therefore, the energy of USMB photons can reach $\sim 100 \text{ GeV}$. Similarly to the case of $E_\gamma^{\max} = 1 \text{ TeV}$, the contributions from USIB photons are important above $\sim 100 \text{ GeV}$. However, such high-energy photons may not reach the Earth, because of duplicated absorption. The optical depth against high-energy photons above $\sim 200 \text{ GeV}$ exceeds unity for $z \sim 0.4$. Hence, the effect of USIB photons will be buried unless GRBs occur at sufficiently low redshifts.

Although we have discussed CIB effects based on fluence $E_\gamma^2 \phi_\gamma$ in Figs. 5 and 6, flux (F_γ) of delayed photons rather than fluence ($E_\gamma \phi_\gamma = \int dt F_\gamma$) is often used in discussing detectability of such photons. Hence, in Figs. 7 and 8, we show fluxes that are numerically obtained for a source at $z = 0.1$. For reference, approximate results obtained by using Eq. (4) are also plotted. The delayed time scale is evaluated using Eqs. (1)-(3). In both Figs. 7 and 8, the small difference between the numerical results and the approximate ones using Eq. (4)

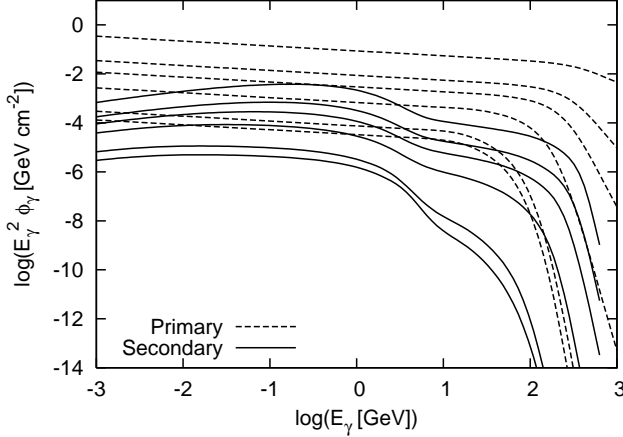


FIG. 5.— The overall fluences of primary and secondary gamma-rays for model A ($E_{\gamma}^{\max} = 1$ TeV). Redshifts (from top to bottom) are $z = 0.1$, $z = 0.3$, $z = 0.5$, $z = 1$, $z = 3$ and $z = 5$.

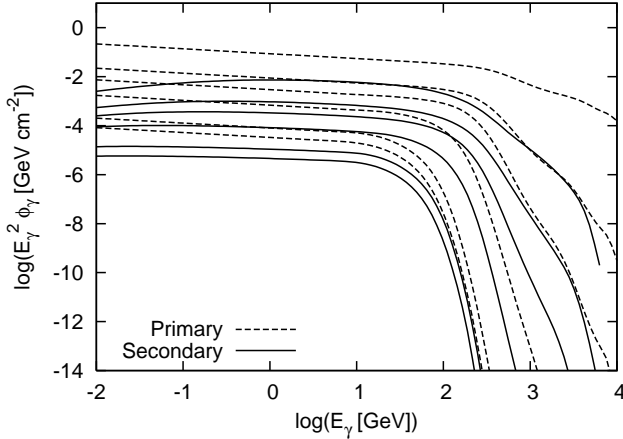


FIG. 6.— The same as Fig. 5, but for model B ($E_{\gamma}^{\max} = 10$ TeV).

is seen around the peak of the bump formed by USMB photons. This difference will be caused by cooled electrons, as explained below. The approximation using Eq. (4) means that both pair creation and IC scattering are treated as entirely local processes. But high-energy electrons will be produced after passing $\sim \lambda_{\gamma\gamma}$ and IC scattering will occur after passing $\sim \lambda_{IC} = c\hat{t}_{IC}$. Thus, these propagating electrons suffer from IC losses as well as adiabatic losses and effective electron distribution would deviate from the expression in Eq. (5). Photon emissivity will be also changed correspondingly, and the difference between two methods appears. For example, the peak of the USMB bump becomes more ambiguous due to such losses. Nevertheless, the approach to use Eq. (4) will usually work as a reasonable approximation.

As is shown in Fig. 7 ($E_{\gamma}^{\max} = 1$ TeV), delayed emissions in $\sim (10-100)$ GeV due to USIB photons are prominent. In this case, the treatment neglecting the USIB effect is not good and leads to underestimation of the delayed gamma-ray flux. Even for $E_{\gamma}^{\max} = 10$ TeV (see Fig. 8), the USIB effect is still remarkable. In fact, the contribution from USIB photons is dominant above ~ 500 GeV. However, the USIB effect is smaller than the case of $E_{\gamma}^{\max} = 1$ TeV, since a fraction of delayed secondary photons is absorbed again by CIB photons.

USMB photons form the “bump” shape around the $E_{\gamma} \sim \text{a few } \times \gamma_e^2 \epsilon_{CMB}/(1+z)$, resembling the Planck distribution.

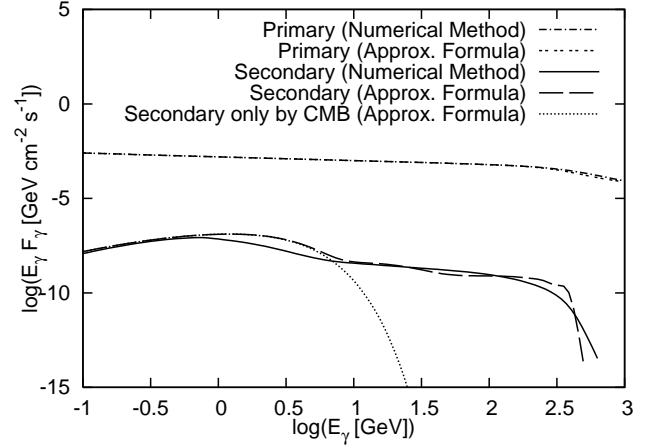


FIG. 7.— Flux for model A ($E_{\gamma}^{\max} = 1$ TeV) obtained numerically and obtained using Eq. (4). The redshift of a source is set to $z = 0.1$. The primary flux is evaluated for the intrinsic GRB duration $T' = 50$ s (i.e. time-averaged flux over the duration is assumed). On the other hand, the delayed secondary flux is evaluated at the observation time $t = 10^4$ s (i.e. the flux which is essentially time-averaged over $t = 10^4$ s is assumed).

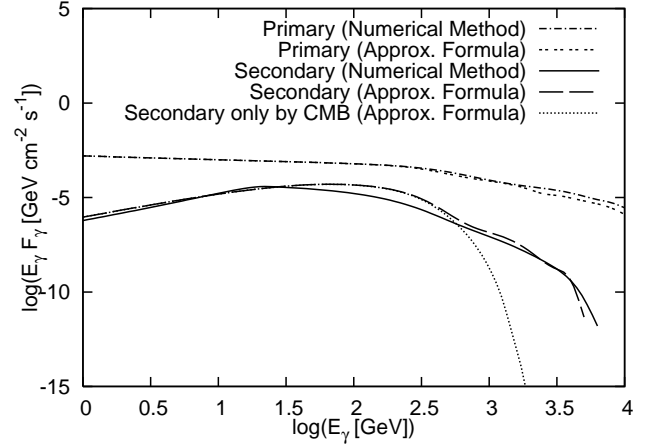


FIG. 8.— The same as Fig. 7, but for model B and the observation time $t = 10^2$ s.

Unless duplicated absorption of secondary photons is significant, the ratio of the fluence due to USIB photons to that due to USMB photons should reflect the ratio of the CIB energy density to the CMB energy density. This statement is basically demonstrated in Fig. 9, from which we can see that $E_{\gamma}^2 \phi_{\gamma}$ at 100 GeV is about 0.01 times lower than that at 1 GeV for the normal CIB strength, when the burst occurs at $z = 0.1$. However, for the sufficiently high z bursts, the duplicated absorption of secondary photons becomes significant, where the fluence ratio will largely deviate from the ratio of the CIB intensity to CMB one. This implies that we need delayed gamma-ray spectra over wide energy ranges in order to see the USIB effect on the delayed spectra, since the cutoff of delayed secondary emission depends on the CIB strength and the distance to the burst. Note that the number of CMB photons increases at high redshifts, while that of CIB photons does not change monotonically. Therefore, USMB photons are more prominent for bursts at high redshifts.

In model C, the amount of prompt TeV photons is much less than that in model A, and the spectrum of primary prompt emission is not expressed as a simple power-law. Nevertheless, the ratio of $E_{\gamma}^2 \phi_{\gamma}$ in model C is similar to that in model A. Thus, the 100 GeV-1 GeV ratio for low redshift bursts is

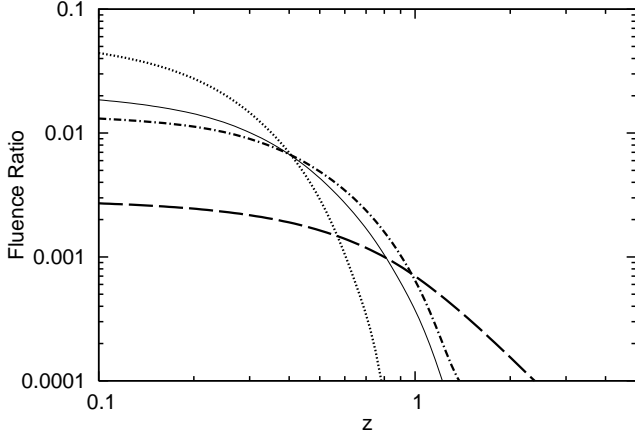


FIG. 9.— The ratio of $E_\gamma^2 \phi_\gamma$ at 100 GeV to that at 1 GeV. The thick dot-dashed line shows the energy fluence ratios for model A and the thin solid line shows those for model C in the normal CIB case, where the best-fit model given by Kneiske et al. (2004) is used. The dashed and dotted lines show the ratios for model A in the stronger CIB case (5 times as strong as the normal case) and weaker CIB case (0.2 times), respectively.

a good indicator of the CIB strength irrespective of the spectral shape of prompt emissions, unless the amount of photons above TeV is considerable.

In Figs. 10 and 11, we show time-integrated fluxes, i.e., fluences at a given time for the model A from sources at $z = 0.1$ and $z = 1$, respectively. In both figures, we change the overall CIB intensity by a factor 5 and 0.2 in order to demonstrate effects of the CIB intensity. As we change the strength of the CIB field, the delayed secondary fluence also changes correspondingly, which is also shown in Fig. 9. For $z = 0.1$, the cosmic space is essentially optically thin for pair creation against CIB photons, so that secondary gamma-rays are not completely absorbed. The USIB effect is outstanding above $\sim (10 - 100)$ GeV range. Even around the bump, where USMB photons are dominant, the fluence changes according to the amount of absorbed primary photons, which reflects the CIB intensity. We can also see the influence of duplicated absorption in the high-energy range, although it is small for the case with $E_\gamma^{\max} = 1$ TeV and $z = 0.1$.

For $z = 1$, delayed secondary spectra become more complicated. Above ~ 70 GeV, gamma-rays cannot reach the Earth without attenuation. Hence, delayed secondary gamma-rays above this energy are absorbed again and regenerated. If we change the strength of the CIB field (as represented in the dotted or dashed line in Figs. 10 and 11), the cutoff energy, at which the optical depth becomes $\tau_{\gamma\gamma}^{\text{bkg}} = 1$, also changes. Although the height of the USMB bump is also affected by the CIB intensity, this influence will be saturated when primary gamma-rays are completely attenuated, like in the cases shown in Fig. 11.

Figs. 12 and 13 show the contrastive results among the three models. For low redshift bursts as shown in Fig. 12, the high-energy slope feature is produced by the CIB for all the models. For high redshift bursts, such high-energy USIB slope appears for model A and model C, which is shown in Fig. 13. For model C, although a bump signature formed by USMB photons is difficult to be seen, the USIB effect is still important and delayed secondary photons above ~ 5 GeV comes mainly from such USIB photons. On the contrary, in the case of model B, USIB photons are almost completely absorbed again. Hence, the contribution of USIB photons is negligible and it is sufficient to consider USMB photons only

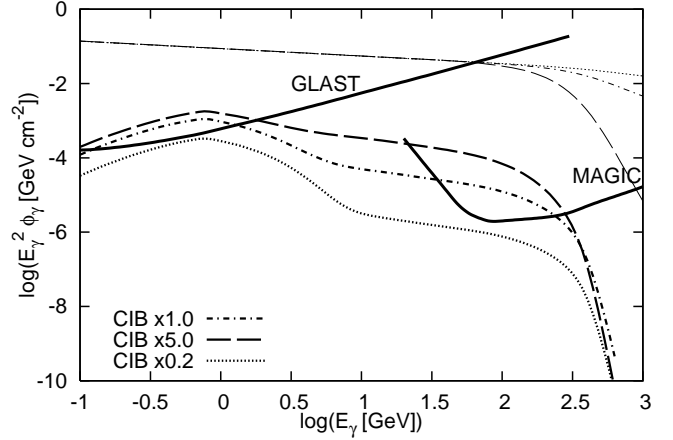


FIG. 10.— The fluences of primary and secondary gamma-rays. Model A with the redshift $z = 0.1$ is used. Fluences of prompt primary (upper three thin lines) and delayed secondary emission (lower three thick lines) are time-integrated over $T' = 50$ s and $t = 10^4$ s, respectively. The CIB strength is assumed to be normal (the best-fit model, dot-dashed), stronger (5 times, dashed), and weaker (0.2 times, dotted).

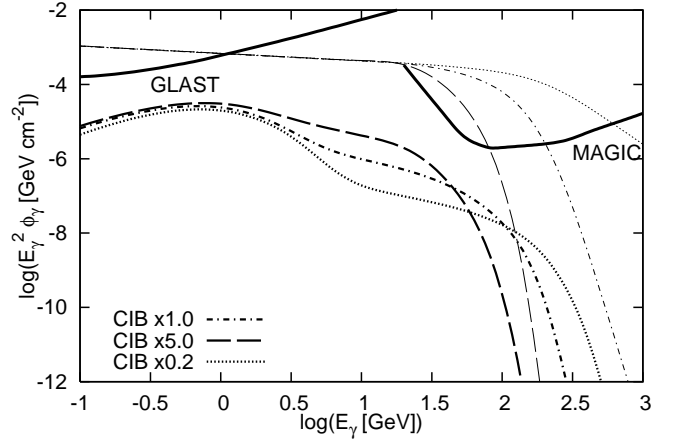


FIG. 11.— The same as Fig. 10, but for $z = 1$.

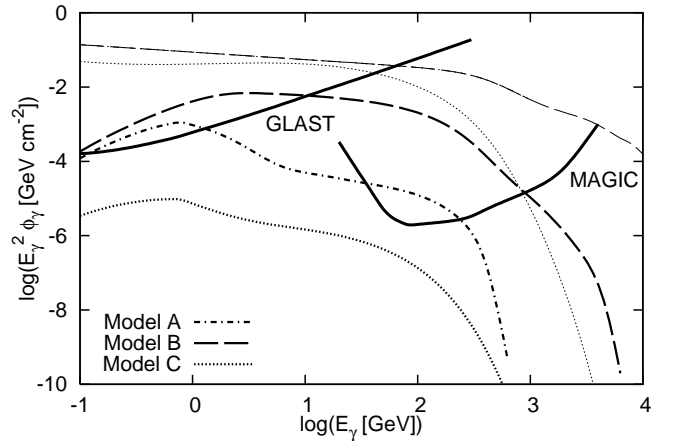


FIG. 12.— The same as Fig. 10, but for models A, B and C with normal CIB strength. The dot-dashed and dotted lines are degenerate for prompt primary spectra.

in this case.

In Figs. 10-13, we have also shown the short-time sensitivity curves of GLAST and MAGIC just for comparison.

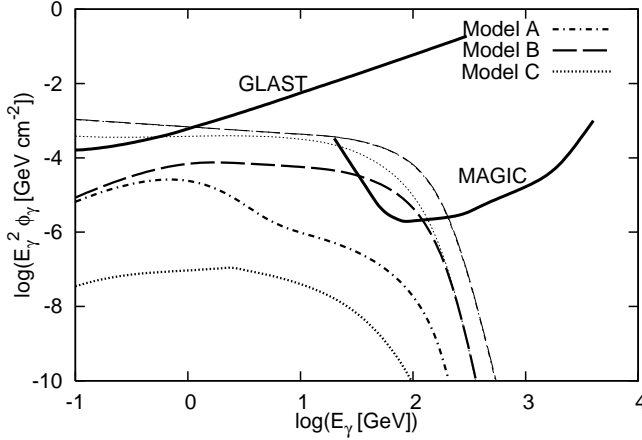


FIG. 13.— The same as Fig. 12, but for $z = 1$. The dot-dashed and dotted lines are degenerate for prompt primary spectra.

For GLAST, the fluence threshold is roughly proportional to $(t/2.4 \times 10^4 \text{ s})^{1/2}$ for the long-time sensitivity regime (exposure time $t \gtrsim 2.4 \times 10^4 \text{ s}$), and is roughly constant for the short-time sensitivity regime (exposure time $t \lesssim 2.4 \times 10^4 \text{ s}$). The short-time sensitivity is calculated from the effective area of LAT onboard GLAST (which is shown in “http://www-glast.slac.stanford.edu/software/IS/glast_lat_performance.htm”), under the criterion that at least 5 photons are collected (Kamae 2006, Private Communication). Note that the GLAST sensitivity curves shown in some references (Petty et al. 1999; Razzaque et al. 2004) are overestimated. For MAGIC, the short-time sensitivity is roughly estimated from the effective area for the zenith angle with 20 degree by the criterion that at least 10 photons are collected, although the actual detectability requires careful analyses (MAGIC Collaboration 2006b). In addition, the duration time of delayed signals can be much longer than that of prompt signals. For such long lasting signals, we have to take into account the fact that the fluence sensitivity is proportional to $t^{1/2}$ for the long-time sensitivity regime.

For 10^{53} ergs bursts at $z = 0.1$, delayed signals can be detected by GLAST for model A and model B. In addition, the USIB effect around (10–100) GeV in delayed emissions could be detected by MAGIC if the CIB strength is strong enough.

Even for the case of $z = 1$, MAGIC and GLAST have possibilities to detect prompt primary signals (although MAGIC has not observed such high-energy emission up to now), if GRBs with 10^{53} ergs are $\sim 10 \text{ GeV} - 10 \text{ TeV}$ emitters. However, even GLAST could not see delayed secondary components for $z \gtrsim 1$ unless bursts are much more energetic. This result is different from that of Razzaque et al. (2004). This discrepancy comes from just their overestimation of the GLAST sensitivity. Only energetic and/or low redshift bursts allow GLAST to detect secondary delayed signals from GRBs.

3.2. Diffuse Gamma-Ray Background

In the previous section, we have considered the weak IGM field case. Here, let us consider the opposite case, where secondary gamma-rays contribute to the diffuse gamma-ray background. Fig. 14 shows the resulting diffuse background in the sense of cumulative gamma-ray background. Even if the primary photons are assumed to contribute to the diffuse background, the contribution is much smaller than the

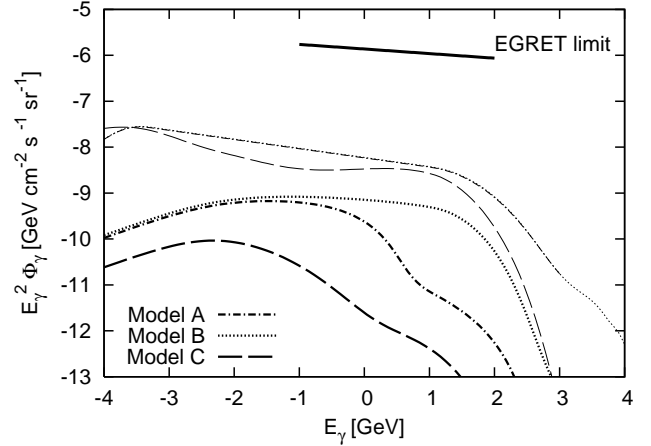


FIG. 14.— The possible diffuse gamma-ray background from GRBs for each model. It is assumed that the GRB rate traces the SF2 model with the local rate $\rho_{\text{GRB}} = 1 \text{ Gpc}^{-3} \text{ yr}^{-1}$. Note that the contribution from delayed secondary emission is expected to be smaller than that from prompt primary one. The dot-dashed and dotted lines are degenerate for prompt primary spectra.

EGRET limit. The contribution due to delayed emissions is much less important. This is easily understood as follows. If we assume the local GRB rate ρ_{GRB} (without beaming correction) $\sim 1 \text{ Gpc}^{-3} \text{ yr}^{-1}$ and the released isotropic energy $E_{\text{iso}} \sim 10^{53}$ ergs, the Hubble time t_H ($\sim 10^{10}$ yr) and the possible cosmological evolution factor on the rate leads to the diffuse background $E_\gamma^2 \Phi_\gamma \sim (1/4\pi)cE_{\text{iso}}\rho_{\text{GRB}}(z=1)t_H \sim 10^{-7} \text{ GeV cm}^{-2} \text{ s}^{-1} \text{ sr}^{-1}$, which is much smaller than the EGRET limit $\sim 10^{-6} \text{ GeV cm}^{-2} \text{ s}^{-1} \text{ sr}^{-1}$ at GeV. Hence, the contribution from GRBs to gamma-ray background is expected to be at most $\sim 10\%$.

4. SUMMARY AND DISCUSSION

In this paper, we have studied the delayed secondary emission in detail. We have evaluated delayed GRB spectra in most detail by numerical simulations, which enable us to treat cascade processes including multiple pair creation and IC scattering. We have also calculated delayed GRB spectra using Eq. (4) and compared both results. As seen in the previous section, both methods agree with each other basically.

We have especially focused on effects of the CIB. CIB photons play a role not only on absorbing high-energy gamma-rays but also on being up-scattered as seed photons by created high-energy pairs. USIB photons have larger energy than USMB photons, so that USIB photons are more subject to duplicated absorption by CIB photons. The USIB component is more sensitive to the CIB than the USMB component. One of the most frequently discussed method to probe the CIB is measuring the depletion due to the CIB in prompt GRB spectra. However, owing to uncertainties in GRB intrinsic spectra, the depletion is hard to be estimated. On the other hand, the USIB signature could be more useful to probe the CIB almost irrespective of intrinsic GRB spectra as shown in Fig. 9 for models A and C. While we focus on secondary emissions from GRBs, secondary emissions from blazars are more expected (Aharonian et al. 1994; Dai et al. 2002; Fan et al. 2004). Our results can be also applied to blazars and effects of the CIB can be important.

In this paper, we have clarified the USIB effect especially. As shown in Figs. 10–13, not only GLAST but MAGIC and VERITAS could detect such high-energy gamma-rays arising from USIB photons for sufficiently low redshift bursts. There are several characteristic features related to USIB pho-

tons: (1) The USIB signature such as high-energy slope appears for bursts with the sufficiently low intrinsic high-energy cutoff E_{γ}^{\max} and/or sufficiently low redshift. (2) If (1) is satisfied (which means duplicated absorption can be neglected), the ratio of the USIB component to the USMB one basically reflects the ratio of the CIB energy density to the CMB one. (3) The cutoff of delayed spectra is sensitive to the CIB, because secondary photons can also be absorbed by CIB photons again. Therefore, the energy range, in which USIB photons are prominent, becomes narrower, as the source redshift becomes higher. (4) As long as the effective intrinsic high-energy cutoff E_{γ}^{\max} is smaller than TeV, the shape of delayed secondary spectra, especially the 100 GeV-GeV ratio, is not so sensitive to the shape of prompt primary spectra. For example, high-energy USIB slope can be found in both model A and model C as seen in the previous section.

It is important to know the highest energy of gamma-rays. These gamma-rays, which may arise from electron synchrotron radiation, electron SSC, proton synchrotron and particles generated by photomeson or photopair production, will suffer from absorption due to electron-positron pair creation. Numerical simulations in Asano & Inoue (2007) show that the intrinsic high-energy cutoff determined by photon absorption is approximated as

$$E_{\gamma}^{\max} \approx 10^9 \left(\frac{\Gamma}{100} \right)^4 \left(\frac{E_{\text{sh}}}{10^{51} \text{ ergs}} \right)^{-0.5} \left(\frac{\delta t}{1 \text{ s}} \right)^{1.3} \text{ eV}, \quad (13)$$

where δt is the variability time scale in prompt emission. Hence, it is possible to constrain a bulk Lorentz factor by observing the highest gamma-ray energy. However, the highest gamma-ray energy can be seen in the prompt spectrum only if attenuation due to the CIB is not significant. Because delayed secondary emission is also influenced by the highest gamma-ray energy (for example, the typical energy of the USMB bump is affected by the intrinsic high-energy cutoff E_{γ}^{\max}), observations of these delayed signals could provide us with useful information on the source.

Now, MAGIC has continued observations and given upper limits for some events (MAGIC Collaboration 2006a; MAGIC Collaboration 2006b). Upper limits are also set by other detectors such as Whipple (Connaughton et al. 1997) and STACEE (Jarvis et al. 2005). So far, no excess event above ~ 100 GeV was detected, neither during the prompt emission phase nor during the early afterglow. The upper limits between 85 and 1000 GeV are derived and compatible with a naive extension of power-law spectra.

As we have discussed, the USIB signature in delayed spectra can be found for GRBs with the relatively low redshift and/or relatively low high-energy cutoff. For example, the rate of GRBs within $z = 0.2 - 0.3$ is $\sim \text{a few yr}^{-1}$, so that we could see such delayed signals by detectors such as MAGIC in the near future. However, the event rate would be not so large. The various conditions such as a field of view and observational conditions of the detector will reduce the expected event rate significantly. Furthermore, the real rate may be smaller because the number of bursts that can emit such high-energy gamma-rays may be limited. GLAST will see the significant number of GRBs emitting high-energy gamma-rays and provide us with information on high-energy spectra of prompt emission. In addition, by using GLAST as the monitor of GRBs that emit high-energy gamma-rays, opportunities to observe high energy gamma-rays by ground telescopes will also be increased. Since GLAST may see many bursts, some of which may include ones with delayed $\sim \text{GeV}$ components.

Furthermore, MAGIC-II is now being constructed and VERITAS has started observations. These advances in detectors could enable us to expect more and more chances to high-energy gamma-ray signals from GRBs.

Here, we discuss possible complications. One is possible influence of environments around GRBs. We have neglected effects of the environments around host galaxies. But, there might be influences from environments such as magnetic field of the host galaxies. The second is the existence of the IGM field. In this paper, we have assumed the weak IGM field with $B \lesssim 10^{-(18-19)} \text{ G}$ to estimate delayed secondary fluxes, where the magnetic deflection time is not a dominant time scale and the angular-size spreading of delayed gamma-rays is sufficiently small. Although such a weak magnetic field might be possible in the void region, it becomes difficult to observe delayed signals when the IGM field is strong enough. This is also the reason why the orphan delayed emission (which can be expected when $\theta_B \gtrsim \theta_j$) is difficult to be detected. Especially for $B \gtrsim 10^{-16} \text{ G}$, delayed secondary photons will be observed as isotropic diffuse signals that are difficult to be observed.

The third possible complication would arise from prolonged intrinsic high-energy emission. TeV signals are also expected in the context of the afterglow theory. Although the discrimination might be difficult, time-dependent observations could enable us to distinguish between two signals, because the time evolution will be different between the prompt emission and afterglow emission. Other possible late activities discovered by Swift would make further contamination. For example, flares can be accompanied not only by neutrinos and gamma-rays associated with flares themselves (Murase & Nagataki 2006b) but also by gamma-rays which forward shock electrons up-scatter (Wang et al. 2006).

Finally, we shall comment on high-energy emissions from low-luminosity (LL) GRBs. The recent discovery of XRF 060218 (Campana et al. 2006) implies that there may be a different population from usual cosmological high-luminosity (HL) GRBs. These LL GRBs are more frequent than usual HL GRBs. If true, the high-energy neutrino background from LL GRBs can be comparable with that from HL GRBs (Murase et al. 2006; Gupta & Zhang 2007). Similarly, we can expect the gamma-ray background from LL GRBs is comparable with that from HL GRBs. This is also pointed out by Casanova et al. (2007) and Dermer (2006). However, the diffuse gamma-ray background from GRBs is much smaller than the EGRET bound and the diffuse component will be very difficult to be detected. Furthermore, it might be difficult to emit TeV photons from LL GRBs, unless they have large Lorentz factors. Although we cannot deny the possibility for LL GRBs to emit TeV photons so far, we do not consider such cases in this paper.

In summary, we have done the most detailed numerical calculations, and justified the frequently used approximate approach. We have especially studied CIB effects on delayed gamma-ray spectra from GRBs in detail. CIB photons are important because primary TeV gamma-rays are absorbed by them. In addition, we have emphasized that not only CMB photons but also CIB photons will be up-scattered by produced electron-positron pairs, and enable delayed secondary spectra to extend to higher energies. Although this USIB effect has not been emphasized in previous studies, it is important since we could obtain additional information on the CIB.

We thank T. Kneiske for giving us advice to use their CIB spectral model. K.M. thank T. Totani. and K. Ioka for comments on effects of the CIB. K.M. and S.N. also thank J. Granot, T. Kamae and M. Teshima for helpful comments. K.M. and K.A. thank S. Inoue for helpful discussion. We are grateful to Z.G. Dai and Y.Z. Fan for useful advices. We would like to appreciate for the anonymous referee for giving us prof-

itable suggestions.

This work is supported by the Grant-in-Aid for the 21st Century COE "Center for Diversity and Universality in Physics" from the Ministry of Education, Culture, Sports, Science and Technology (MEXT) of Japan. The work of K.M. is supported by a Grant-in-Aid for JSPS Fellows.

REFERENCES

- Aharonian, F.A. et al. 1994, *ApJ*, 423, L5
 Aharonian, F.A. et al. 2006, *Nature*, 440, 1018
 Amenomori, M. et al. 2001, *AIPC. Proc.*, 599, 493
 Ando, S. 2004, *MNRAS*, 354, 414
 Asano K. 2005, *ApJ*, 623, 67
 Asano, K., and Inoue, S. 2007, *arXiv:0705.2910*
 Asano, K., and Nagataki, S. 2006, *ApJ*, 640, L9
 Asano, K., and Takahara, F. 2003, *PASJ*, 55, 433
 Atkins, R. 2000, *ApJ*, 533, L119
 Blumenthal, G.R., and Gould, R.J. 1970, *Rev. Mod. Phys.*, 42, 237
 Bruzual, A. G., and Charlot, S. 1993, *ApJ*, 405, 538
 Campana, et al. 2006, *Nature*, 442, 1008
 Casanova, S., Dingus, B., and Zhang, B. 2007, *ApJ*, 656, 306
 Cheng, L.X., and Cheng, K.S. 1996, *ApJ*, 459, L79
 Connaughton, V. et al. 1997, *ApJ*, 479, 859
 Dai, Z. G., Zhang, B., Gou, L. J., Meszaros, P., and Waxman, E. 2002, *ApJ*, 580, L7
 Dai, Z.G., and Lu, T. 2002, *ApJ*, 580, 1013
 Dermer, C.D. 2006, *astro-ph/0610195*
 Dermer, C. D., & Atoyan, A. 2003, *Phys. Rev. Lett.*, 91, 071102
 Dermer, C.D., and Atoyan, A. 2004, *A&A*, 418, L5
 Dermer, C.D., Chiang, J., and Mitman, K. 2000, *ApJ*, 537, 785
 Derishev, E. V., Kocharovsky, V. V., and Kocharovsky, V. V. 2001, *A&A*, 372, 1071
 Enomoto, R. et al. 2002, *Astropart. Phys.* 16, 235
 Fan, Y. Z., Dai, Z. G., Wei, D. M. 2004, *A&A*, 415, 483
 Guetta, D., Spada, M., & Waxman, E. 2001, *ApJ*, 559, 101
 Guetta, D., and Granot, J. 2003, *ApJ*, 585, 885
 Guetta, D., Hooper, D., Alvarez-Muñiz, J., Halzen, F., & Reuveni, E. 2004, *Astropart. Phys.*, 20, 429
 Guetta, D., Perna, R., Stella, L., and Vietri, M. 2004, *ApJ*, 615, L73
 Guetta, D., and Piran, T. 2007, *JCAP*, 07, 003
 Gupta, N., and Zhang, B. 2007, *Astropart. Phys.*, in press
 Hartmann, D.H. et al. 2002, *AIPC. Proc.*, 662, 477G
 Hauser, M.G., and Dwek, E. 2001, *ARA&A*, 39, 249
 Hinton, J.A. 2004, *New Astron. Rev.*, 48, 331
 Holder, J. et al. 2006, *astro-ph/0611598*
 Hurley, K. et al., 1994, *Nature*, 372, 652
 Jarvis, B. et al. 2005, *Proc. of the 29th International Cosmic Ray Conference*, 4, 455
 Kamae, T. 2006, Private Communication
 Kashlinsky, A. 2006, *New Astron. Rev.*, 50, 208
 Kneiske, T.M., Mannheim, K., and Hartmann, D.H. 2002, *A&A*, 386, 1
 Kneiske, T.M. et al. 2004, *A&A*, 413, 807
 Le, T., and Dermer, C.D. 2007, *ApJ*, 661, 394
 Liang, E. et al. 2007, 662, 1111
 Lithwick, Y., and Sari, R. 2001, *ApJ*, 555, 540
 MAGIC Collaboration, 2006, *ApJ*, 641 L9
 MAGIC Collaboration, 2006, *astro-ph/0612548*
 Mészáros, P. 2006, *Rep. Prog. Phys.*, 69, 2259
 Mészáros, P., Rees, M. J. 1994, *MNRAS*, 269, L41
 Mészáros, P., Rees, M. J., Papathanassiou, H. 1994, *ApJ*, 432, 181
 Milagro Collaboration 2007, *arXiv:0705.1554*
 Mirzoyan et al. 2005, *Proc. of the 29th International Cosmic Ray Conference*, 4, 23
 Murase, K., and Nagataki, S. 2006a, *Phys. Rev. D*, 73, 063002
 ———. 2006b, *Phys. Rev. Lett.*, 97, 051101
 Murase, K., Ioka, K., Nagataki, S., and Nakamura, T. 2006, *ApJ*, 651, L5
 Papathanassiou, H., and Meszaros, P., *ApJ*, 471, L91
 Peer, A., and Waxman, E. 2004, *ApJ*, 613, 448
 Petry, D. et al. 1999, *A&A*, 138, 601
 Poirier, J. et al. 2003, *Phys. Rev. D*, 67
 Porciani, C., and Madau, P. 2001, *ApJ*, 548, 522
 Plaga, R. 1995, *Nature*, 374, 30
 Razzaque, S., Mészáros, P., and Zhang, B. 2004, *ApJ*, 613, 1072
 Sreekumar, P. et al. 1998, *ApJ*, 494, 523
 Stecker, F.W., de Jager, O.C., and Salamon, M.H. 1992, *ApJ*, 390, L49
 Stecker, F.W., Malkin, M.A., and Scully, S.T. 2006, *ApJ*, 648, 774
 Sommer, M. 1994, *ApJ*, 422, L63
 Strong, A.W., Moskalenko, I.V., and Reimer, O. 2004, *ApJ*, 648, 774
 Totani, T. 1998, *ApJ*, 509, L81
 Totani, T., and Takeuchi, T.T. 2002, *ApJ*, 570, 470
 Wang, X.Y., Dai, Z.G., and Lu, T. 2001, *ApJ*, 556, 1010
 Wang, X.Y., Cheng, K.S., Dai, Z.G., and Lu, T. 2004, *ApJ*, 604, 306
 Wang, X.Y., Li, Z., and Mészáros, P. 2006, *ApJ*, 641, L89
 Waxman, E. and Bahcall, J. 1997, *Phys. Rev. Lett.*, 78, 2292
 Zhang, B. 2007, *ChJAA*, 7, 1
 Zhang, B., and Mészáros, P. 2001, *ApJ*, 559, 110